Earth and Planetary Science Letters 387 (2014) 89–96

Contents lists available at ScienceDirect

Earth and Planetary Science Letters

www.elsevier.com/locate/epsl

Reproducing the supershear portion of the 2002 Denali earthquake rupture in laboratory

M. Mello [a], H.S. Bhat [b,*], A.J. Rosakis [c], H. Kanamori [d]

[a] School of Aerospace Engineering, Georgia Institute of Technology, USA
[b] Institut de Physique du Globe de Paris, UMR 7154 CNRS, 1 rue Jussieu, Paris 75005, France
[c] Graduate Aerospace Laboratories, California Institute of Technology, USA
[d] Geological and Planetary Sciences, California Institute of Technology, USA

ARTICLE INFO

Article history:
Received 7 June 2013
Received in revised form 12 November 2013
Accepted 13 November 2013
Available online xxxx
Editor: P. Shearer

Keywords:
supershear earthquake
laboratory earthquakes
trailing Rayleigh pulse
dynamic rupture

ABSTRACT

A notable feature of the 2002 M_w 7.9 Denali, Alaska, earthquake was that a unique set of near-field seismic ground motion records, at Pump Station 10 (PS10), captured the passage of a supershear rupture followed by what was surmised to be a secondary slip pulse, 'Trailing Rayleigh Pulse' (Dunham and Archuleta, 2004; Mello et al., 2010). Motivated by the unique features contained in these near-field ground motion records, which were obtained only 3 km away from the fault, a series of scaled laboratory earthquake experiments was conducted in an attempt to replicate the dominant features of the PS10 ground motion signatures. Particle velocity records bearing a striking similarity to the Denali ground motion records are presented and discussed. The success of the comparison opens up the possibility of routinely generating near source ground motion records in a scaled and controlled laboratory setting that could be of great societal interest towards assessing seismic hazard from large and potentially devastating earthquakes.

1. Introduction

The nature of near fault ground motion associated with a large strike-slip earthquake is of great interest to earthquake engineers and to earth scientists alike because there are few observations with which to constrain either empirical or theoretical models (Ellsworth et al., 2004a). The 2002 (M_w 7.9) Denali fault earthquake provided a unique ground motion record close to the source, at Pump Station 10 about 3 km away from the fault. Another unique feature was that this station recorded the passage of a supershear earthquake rupture (earthquake whose rupture speed exceeds the shear wave speed of the surrounding solid; Rosakis, 2002; Rosakis et al., 2007) providing the only reliable near-source record of such an event. Supershear ruptures are expected to be more destructive since they manifest shear shock wave fronts (Rosakis, 2002; Mello et al., 2010). As a consequence the ground motion associated with supershear ruptures does not attenuate, with distance, as fast as that associated with sub-shear ruptures, sub-Rayleigh in 2D, (Rosakis, 2002; Dunham and Archuleta, 2005; Das, 2007; Rosakis et al., 2007; Dunham and Bhat, 2008; Mello et al., 2010). This doubly important nature of the 2002 Denali event recorded at Pump Station 10 has motivated the present study whose purpose was to recreate such a record in the laboratory earthquake setup (Xia et al., 2004; Rosakis et al., 2007; Mello et al., 2010), using carefully constructed scaling arguments. This opens up the potential to routinely generate near-source strong ground motion records in a controlled laboratory earthquake setting. In addition to its scientific value, this study has an important implication for the response and integrity of buildings near a major fault. For example, the probability of a major earthquake occurring on the southern San Andreas fault in the next 30 years is considered high, and its effect will be felt by large population centers in southern California (Field et al., 2009). This study provides a solid physical framework for generating realistic near-field ground motions.

2. Background

The 2002 (M_w 7.9) Denali fault earthquake was the largest strike-slip rupture to take place on the North American continent in over 150 years and was comparable in magnitude, if not rupture length, only to the 1906 (M_w 7.8) San Francisco earthquake and the 1857 (M_w 7.9) Fort Tejon earthquake. Its total rupture length of 334 km, average slip of 4.9 m, and maximum slip of 8.8 m, ranks it amongst the largest shallow-crust earthquakes recorded anywhere in the world throughout the past two centuries (Haeussler et al., 2004; Bouchon et al., 2010). Due to its remote location within south-central Alaska, there was very little damage to modern infrastructure and fortunately no loss of human life. Field evidence and ground motion data from this event have, however, provided

* Corresponding author.
E-mail address: bhat@ipgp.fr (H.S. Bhat).

0012-821X/$ – see front matter
http://dx.doi.org/10.1016/j.epsl.2013.11.030

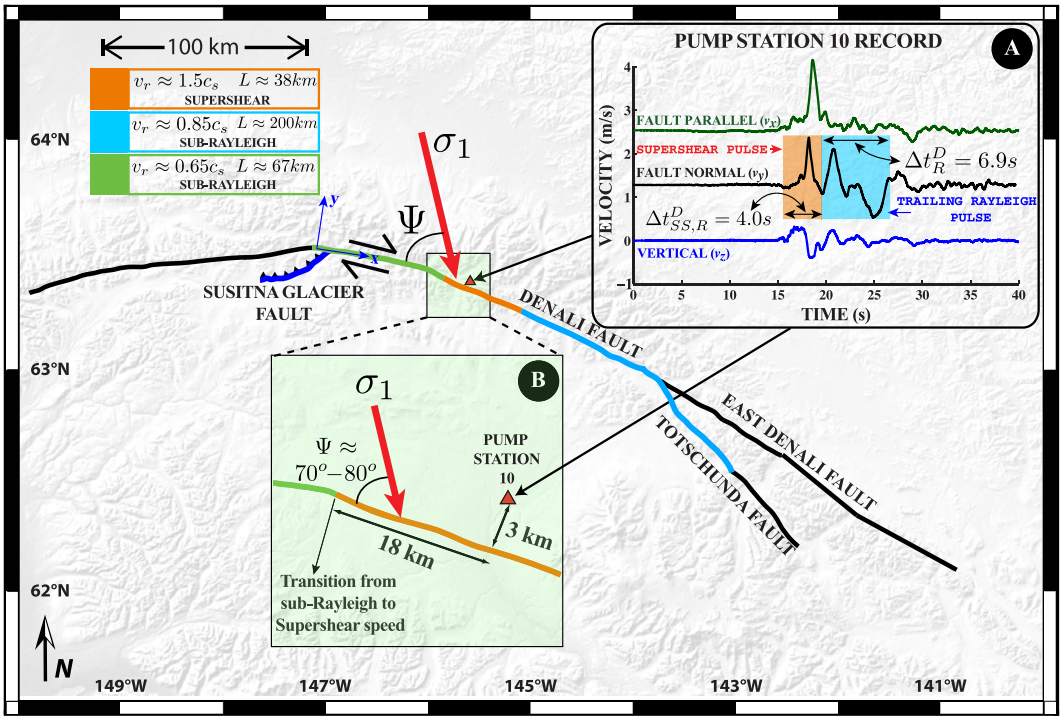

Fig. 1. 2002 M_w 7.9 Denali fault earthquake surface rupture trace annotated with the kinematic inversion results from Ellsworth et al. (2004b). Inset A shows the Pump Station 10 particle velocity records from Ellsworth et al. (2004a) and Inset B shows the region of interest for this work. (For interpretation of the references to color in this figure, the reader is referred to the web version of this article.)

seismologists with a rare and extraordinary opportunity to study a large, shallow crust, strike-slip earthquake, which is in many ways analogous to the major earthquakes which are known to occur along the San Andreas fault (Haeussler et al., 2004).

The Denali earthquake rupture initiated along a 40 km-long segment of the previously unknown Susitna Glacier thrust fault (Fig. 1). The rupture then transferred to the Denali strike-slip fault system and propagated 218 km from west to east along the central Denali fault. The rupture eventually branched off the Denali fault and stepped over onto the Totschunda fault where it propagated for an additional 76 km before finally arresting (Haeussler et al., 2004).

The central Denali fault ruptured beneath the trans-Alaska pipeline (TAP), which crosses the fault, and is located approximately 85 km east of the earthquake epicenter. Close to the TAP–Denali fault crossing a set of "celebrated" near-source ground motion records were obtained at Pump Station 10 (PS10) which is positioned at 63.424 N, 145.763 W along the TAP and is located just 3 km north of the fault. The accelerometer recording station at PS10 is part of the accelerograph network operated by the Alaska Pipeline Service Company. Ellsworth and colleagues (Ellsworth et al., 2004a, 2004b) conducted a thorough analysis and calibration of the PS10 instrumentation and re-processed the signals in order to recover the long-period (>10 s) ground motions. A set of instrument-corrected acceleration, velocity, and displacement time records were obtained and properly rotated into the fault normal (v_y) and parallel (v_x) directions. The fault parallel, fault normal, and vertical (v_z) velocity records are depicted in Fig. 1A.

Forward modeling of the instrument-corrected ground motion records led (Ellsworth et al., 2004a, 2004b) to conclude that a supershear burst occurred along a 38 km segment of the fault, which was nearly centered about PS10. The ground motion records were best matched by their kinematic model if a normalized sub-Rayleigh rupture speed of $V_r/C_s = 0.65$ was assumed over a 67 km stretch between the epicenter and the point of supershear transition. It also predicted that the normalized rupture speed jumped to $V_r/C_s = 1.5$ beyond supershear transition and propagated for a distance of 38 km. This was followed by a decrease to a normalized sub-Rayleigh rupture speed of $V_r/C_s = 0.85$ for points beyond the terminus of the supershear interval (i.e., distances >20 km east of PS10; see Fig. 1). The synthetic records do a reasonable job in capturing the general profile of the leading portions of the FP, FN, and vertical (UP) records although the synthetic vertical curves tend to over-predict the peak vertical ground velocity. The biggest shortcoming of the kinematic model was its inability to capture the prominent secondary pulse in the FN ground motion record which is shaded in blue in Fig. 1. Nevertheless, the careful processing of the instrument-corrected PS10 data and the interpretation of these remarkable ground motion records represent a major seismological finding and the most direct field evidence ever gathered for the existence of a supershear earthquake rupture. The existence of supershear ruptures was conclusively demonstrated in a physical setting in the laboratory earthquake experiments of Rosakis and his co-workers (Rosakis, 2002; Xia et al., 2004; Rosakis et al., 2007) but the Pump Station 10 observations provide one of the most reliable field evidence to their occurrence in the earth's crust.

The numerical investigations of Dunham and Archuleta (2004) noted specific features in the PS10 ground motion records, which they identified as characteristic ground motion signatures of a supershear earthquake rupture. The first unique feature of note involves the existence of a fault parallel (FP) velocity pulse which is approximately 1.5× greater in magnitude than the corresponding fault normal (FN) velocity pulse. The second unique feature is the existence of pronounced velocity swings following the main rupture pulse in the FN record, which (Ellsworth et al., 2004b) was unable to replicate using a simple kinematic model. Dunham and Archuleta (2004) reasoned that the secondary pulses in the FN record resulted from rupture acceleration during the supershear transition and the release of Rayleigh waves during this phase which combine to produce a secondary slip-pulse. This pulse

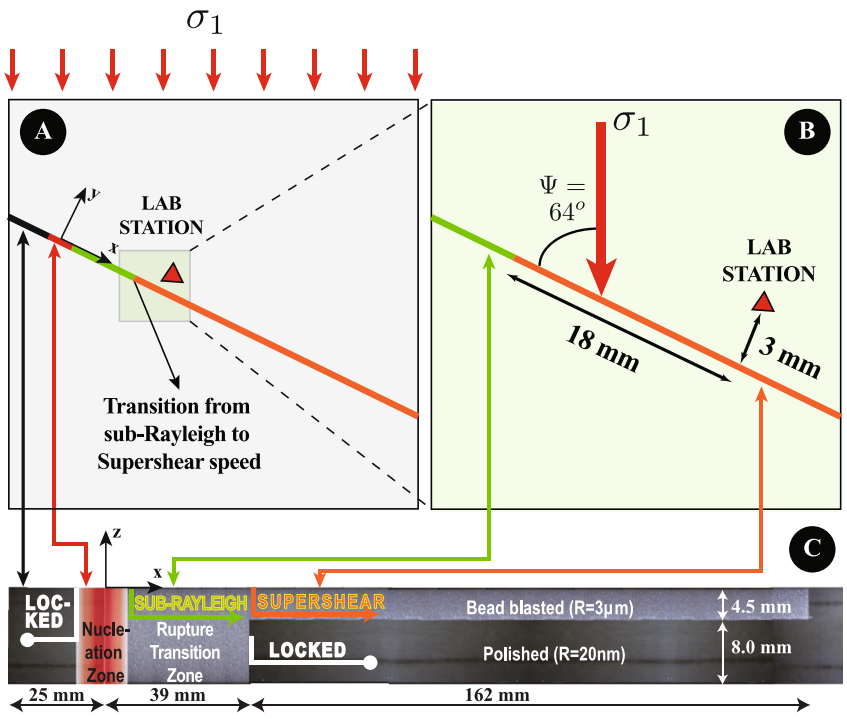

Fig. 2. (A) Schematic of the 3D laboratory specimen hosting a dynamic earthquake rupture along a fault. (B) The region of interest around laboratory station, (x^L, y^L), corresponding to the region depicted in Fig. 1B. (C) Mosaic image of the fault surface depicting the 3D fault geometry. The vertical scale is exaggerated. R corresponds to a root mean squared roughness measure of the bead blasted and polished regions.

trails the primary supershear rupture and propagates at around the Rayleigh wave speed. We will henceforth call this secondary pulse the 'Trailing Rayleigh Pulse'. Both these unique features were confirmed by them using a spontaneous dynamic rupture propagation model which incorporated a slip weakening friction law with a built-in healing mechanism (Nielsen and Carlson, 2000).

Motivated by the success of the dynamic simulations and the physically based interpretation of the secondary slip-pulse, an attempt was made to replicate the most striking features of the PS10 records using the laboratory earthquake arrangement (Xia et al., 2004; Rosakis et al., 2007; Mello et al., 2010). The region of interest that will be modeled experimentally is shown in Fig. 1B. This is an ideal setting because, unlike spontaneous dynamic rupture models, the governing friction law of the interface is naturally 'built-in' and has been shown to have similar features as those for crustal rocks (Rosakis et al., 2007; Lu, 2009).

3. Laboratory earthquake setup

Laboratory earthquake experiments were conducted using 200 mm × 200 mm × 12.5 mm (nominal thickness) Homalite-100 specimen assemblies featuring a 3D fault geometry and a fault oriented at $\Psi = 64°$ with respect to the direction of the compressive principal stress (Fig. 2A, B). Fig. 2C shows specific details of the new 3D specimen fault geometry. This geometry is a 3D extension of the 2D geometry used in past laboratory earthquake studies (Xia et al., 2004; Rosakis et al., 2007). The fault segment to the left of the nucleation site corresponds to a 25 mm × 12.5 mm interface formed by two polished surfaces. The intent is to inhibit rupture propagation to the left through contact bonding of the flat polished surfaces of a short fault segment under the applied static compressive load. The 39 mm roughened fault segment to the right of the polished section provides lower frictional resistance than the polished section and is referred to as the nucleation and rupture transition zone. A NiCr filament channel is milled within 0.5 mm of the boundary between the short polished segment and the nucleation patch on the roughened side of the boundary. A sudden discharge of current through the wire, fluidizes it resulting in a local reduction of normal stress which leads to the nucleation and propagation of an unstable dynamic rupture (Xia et al., 2004; Rosakis et al., 2007). The coordinates $(L_T, 0) = (39, 0)$ mm correspond to a point on the surface of the specimen, at the end of the nucleation patch, where the roughened portion of the fault is abruptly reduced in width from 12.5 mm to 4.5 mm as depicted in Fig. 2C. At the transition location, $(L_T, 0)$, a stress concentration develops, under applied load. This stress perturbation allows a sub-Rayleigh rupture to accelerate to supershear speed (Dunham et al., 2003; Liu and Lapusta, 2008). The polished part of the fault (of width 8 mm), situated below the roughened part, has a higher frictional resistance and is expected to adhere under an applied static compressive load. The roughened frictional part (top) is meant to mimic the brittle upper crust where earthquakes are typically hosted. The polished bottom part represents the ductile part of the crust which remains essentially locked during an earthquake rupture. A reflective tape strip used to enable the particle velocity measurements (Lu et al., 2007; Mello et al., 2010) was positioned with its lower-right corner at the scaled PS10 location (x^L, y^L). The laboratory station coordinates, denoted by the superscript L, will be determined in the next section. The results from several experiments conducted in advance were also used to estimate that a critical load $\sigma_1 > 30$ MPa is required to trigger a supershear rupture at the desired location $(x = L_T)$.

The scaled PS10 supershear experiment was conducted under a static compressive load of $\sigma_1 = 31$ MPa. Three laser interferometer probe beams were focused on the measurement station at (x^L, y^L) in order to simultaneously monitor the fault parallel (v_x), fault normal (v_y), and vertical (v_z) particle velocity components at this location. Synchronized, high-speed photoelastic images (where the fringes correspond to contours of maximum shear stress change in the medium), obtained every few microseconds, were simultaneously acquired in order to obtain a spatially re-

solved, full field view of the dynamic event (Xia et al., 2004; Mello et al., 2010).

4. Development of a scaling relationship

To develop a reasonable scaling argument to reproduce the PS10 record we address the following three questions. One, what is the appropriate temporal scaling that will translate the laboratory station record (a few 10's of micro-seconds in duration) to the PS10 records (a few 10's of seconds in duration). Two, what is the corresponding location of the laboratory station that would ideally represent the spatial location of PS10 with respect to the Denali fault. Three, what is the appropriate amplitude scaling that would match at least the peak particle velocities of PS10 with the laboratory station.

The simplest scaling argument would be to use the along-strike distance between the station and the supershear transition point, $x - L_T$. Temporal scaling could then be obtained by $(x - L_T)/C_s$, where C_s is the shear wave speed. Spatial scaling could then have been achieved by shrinking uniformly from the Denali scale to the lab scale while maintaining some aspect ratio. This would be a valid scaling argument had the rupture been governed by a solitary pulse as opposed to two closely spaced pulses (supershear rupture pulse and the trailing Rayleigh pulse). Since the elastic wave speeds, or to be precise the difference in the elastic wave speeds, is different for Denali and the laboratory material, Homalite, this would result in different arrival times of the main supershear pulse and the trailing Rayleigh pulse. Therefore, to obtain a scaled record that could be overlapped with the PS10 record one needs to find the right station in the laboratory so that the temporal spacing between the two pulses (supershear and trailing Rayleigh) was reproduced with good fidelity. To achieve this we develop the following scaling argument.

The temporal scale is established by the ratio of the temporal width of the trailing Rayleigh pulse portion of the laboratory fault normal (v_y) record, Δt_R^L, and the corresponding temporal width of the trailing Rayleigh pulse of the actual PS10 fault normal (v_y) ground motion record, Δt_R^D. The superscripts L and D denote 'Laboratory' and 'Denali' records respectively. The temporal scaling factor can then be used to stretch one trailing Rayleigh pulse signature onto the other and vice versa. This approach requires confidence in the repeatability of the temporal width of the trailing Rayleigh pulse obtained, at the same location, in the experiments. Indeed this is found to be quite repeatable provided that specimen preparation procedures and all other critical test conditions remained unchanged. Repeated experiments have yielded a temporal width for the trailing Rayleigh pulse portion of the fault normal record, Δt_R^L, of 17.8 μs. The corresponding temporal width of the trailing Rayleigh pulse portion of the fault normal Denali PS10 record, Δt_R^D is 6.9 s. Consequently, the temporal scaling factor is therefore, $S_T = \Delta t_R^D / \Delta t_R^L = 3.87 \times 10^5$.

Spatial scaling is achieved by solving for a laboratory station position that would give the same difference in arrival times of the main supershear pulse and the secondary trailing Rayleigh pulse at the laboratory station, $\Delta t_{SS,R}^L$, and the PS10, $\Delta t_{SS,R}^D$, after temporal scaling i.e. $\Delta t_{SS,R}^L = \Delta t_{SS,R}^D / S_T = 10.3$ μs. As shown in the supplementary material, the solution to this analytical problem in fact leads to a family of stations, (x, y), described by:

$$y = x \tan\beta - L_* \tag{1}$$

where $\tan\beta$ and L_* will be defined shortly.

Additional geometric scaling is imposed in order to further constrain the infinite set of stations given by Eq. (1). It is assumed that in both cases, Laboratory and Denali, the ratio, S_L, of the fault normal coordinate of the station, y, to the fault parallel distance relative to the supershear transition location, $(x - L_T)$, remain the same i.e.

$$\frac{y^D}{(x^D - L_T^D)} = \frac{3\text{ km}}{18\text{ km}} = \frac{y^L}{(x^L - L_T^L)} = S_L \tag{2}$$

The distances used in calculating the above for PS10 were obtained from Ellsworth et al. (2004a). Substituting the geometric constraint given by Eq. (2) into Eq. (1) yields the PS10 equivalent coordinates on the surface of the laboratory earthquake test specimen.

$$x^L = \frac{L_*^L - L_T^L S_L}{\tan\beta^L - S_L}; \qquad y^L = S_L\left(x^L - L_T^L\right) \tag{3}$$

where,

$$L_*^L = \left(L_T^L + \frac{C_s^L \Delta t_{SS,R}^D}{S_T}\right)\tan\beta^L$$

$$\tan\beta^L = \left(\frac{C_s^L}{C_R^L} - \frac{C_s^L}{V_r^L}\right)\left[1 - \left(\frac{C_s^L}{V_r^L}\right)^2\right]^{-1} \tag{4}$$

Here C_R is the Rayleigh wave speed ($C_R \approx 0.92 C_s$), C_s is the shear wave speed, V_r is the supershear rupture speed ($V_r \geqslant C_s$) and L_T is the transition length which is the distance traveled by the sub-Rayleigh rupture before transitioning to supershear speed. In implementing Eqs. (3), (4) one needs S_L and $\Delta t_{SS,R}^D$ from PS10 record (or any equivalent station), S_T from PS10 record and prior knowledge of the width of the trailing Rayleigh pulse in the laboratory experiments. To finally compute (x_L, y_L) for a particular experimental design, one needs to further set L_T.

Substituting into Eqs. (3), (4) $C_s^L = 1.28$ mm/μs, $L_T^L = 39$ mm, $C_R^L = 0.92 C_s^L$ and $V_r^L = 1.7 C_s$, one obtains $(x^L, y^L) = (57, 3)$ mm. Note that the parameters for L_T^L (Laboratory) is set *a priori* by design and that $V_r \approx 1.7 C_s$ is determined from experimental trials, held under same initial stress and friction states, prior to converging on the final experiment, which is then scaled.

Once the observation station is set and experimental records are obtained they are then subjected to temporal scaling using the relation, $t^{scaled} = t^L \times S_T$. The spatial scaling and geometric constraint used to design the experiment automatically ensures that the arrival times of the supershear and trailing sub-Rayleigh ruptures in the scaled laboratory record will coincide with the arrival times of the equivalent features in the actual PS10 ground motion record.

As a final step, the particle velocity magnitudes are scaled by the peak to peak swing in the trailing Rayleigh pulse part of the record. Based on the steady-state slip-pulse models of Rice et al. (2005), Dunham and Archuleta (2005), Samudrala et al. (2002) the proper non-dimensionalized representation of the velocity field in a medium hosting a slip pulse of length L with a process zone of size R is given by

$$\mathbf{v}\left(\frac{x}{L}, \frac{y}{L}\right) = \hat{\mathrm{v}}_o \mathbf{F}\left(\frac{x}{L}, \frac{y}{L}, \frac{R}{L}, \frac{V_r}{C_s}\right)$$

$$\text{where } \hat{\mathrm{v}}_o = C_s \frac{(\tau_p - \tau_r)}{\mu} \tag{5}$$

where μ is the shear modulus, $\tau_p - \tau_r$ is the strength drop, C_s is the shear wave speed and $\mathbf{v}$ is the in-plane particle velocity vector. This universal feature applies to all elastodynamic rupture models. For a class of models utilizing slip/distance weakening (Rice et al., 2005; Dunham and Archuleta, 2005) and velocity weakening (Samudrala et al., 2002) the actual functional form of $\mathbf{F}$ can be obtained analytically. A typical value for the shear modulus of crustal rock is 30 GPa, while the corresponding value for Homalite-100 is 1.96 GPa. At mid-seismogenic depths (around 7 km) the normal stress σ is estimated to be of the order of 100 MPa. If

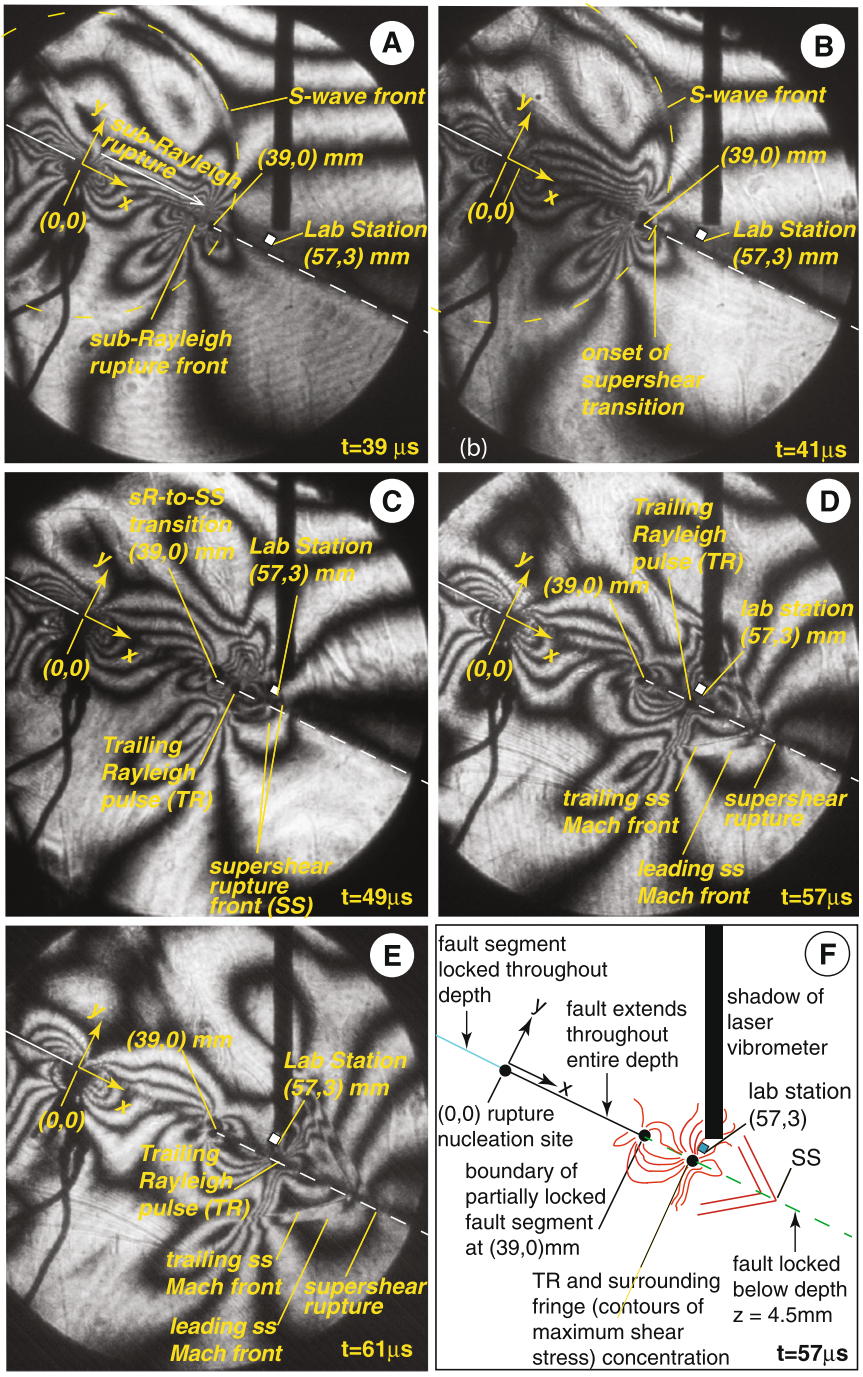

Fig. 3. (A)–(E) Photoelastic images acquired at various stages of the experiment. (F) Schematic explanation of the photoelastic images. SS stands for supershear and TR for trailing Rayleigh. The fringes in the photo elastic images correspond to contours of maximum shear stress induced by the propagating rupture. (For interpretation of the references to color in this figure, the reader is referred to the web version of this article.)

a Coulomb-like friction relation is assumed ($\tau = f\sigma$, where f is the friction coefficient and σ is the normal stress), then assuming $f_p = 0.6$ and $f_r = 0.2$, a strength drop on the order of 40 MPa is obtained for crustal rock. Assuming C_s for crustal rocks is 3.5 km/s the value of the velocity amplitude, $\hat{v}_o$, for rock is 4.67. A typical strength drop in laboratory earthquake experiments is about 7 MPa (assuming a principal stress magnitude of 31 MPa), giving a value of $\hat{v}_o$ close to 4.57, while reasonably assuming R/L and v_r/c_s are similar for rupture in Homalite-100 and crustal rock. It stands to reason therefore, that the particle velocity records obtained in laboratory earthquake experiments should be comparable to the magnitude of ground motion velocities measured in natural earthquakes and thus can be adjusted moderately to match the PS10 record. As stated earlier the actual adjustment is done by using the peak to peak swing of the trailing Rayleigh pulse part of the record.

5. Experimental results

The photoelastic image sequence in Fig. 3 provides a spatially-resolved, frame-by-frame view of the scaled PS10 supershear experiment. The stationary dark, circular caustic zone at $(39, 0)$ mm, indicated in Figs. 3A and C–E, corresponds to the stress concentration at the boundary between the roughened and polished

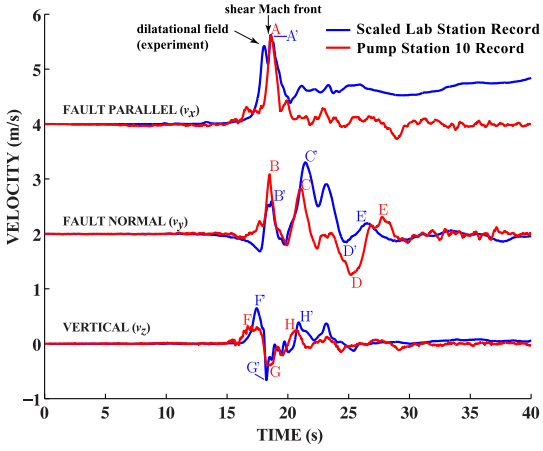

Fig. 4. Scaled laboratory station records compared with the Denali Pump Station 10 record.

(locked) fault segments. The long cylindrical shadow seen in each of the image frames was produced by the side exit probe, which was used to direct the vertical laser interferometer probe beam to the measurement station at $(57, 3)$ mm. Figs. 3A, B depict the sub-Rayleigh rupture as it encountered the boundary of the locked fault segment. The increased diameter of the caustic zone at $(39, 0)$ mm reveals a stress build-up which occurred as the advancing sub-Rayleigh rupture field was superimposed upon the pre-existing static stress field at the boundary of the locked fault segment. A supershear transition was triggered by the locked fault segment, which acted as a high-strength barrier, or, alternatively, as a patch of higher pre-stress (Dunham et al., 2003). The observed supershear transition in the scaled PS10 experiment is notably different than the classical Burridge–Andrews (Rosakis, 2002; Rosakis et al., 2007) type transition mechanism since this transition is artificially induced. Well-formed shear Mach/shock fronts are clearly visible in Figs. 3D, E. The appearance of two shear Mach fronts indicates regions of high gradients in slip velocity traveling with the rupture tip. For a perfect slip pulse these two regions correspond to the leading and the healing edges of the slip pulse. The image frames also capture the trailing Rayleigh pulse, TR, rupture as it sweeps across the off-fault station at $(57, 3)$ mm. The location of TR is indicated in Figs. 3C–E.

The particle velocity records obtained from this experiment are shown in Fig. 3F and Fig. 4. The leading portions of all three of the particle velocity records are dominated by the fault parallel record, as expected to be generated by a supershear rupture front propagating at a speed in excess of $\sqrt{2}c_s$ (Rosakis, 2002; Mello et al., 2010). Also, the fault parallel component features a pronounced double peak at about 50 μs. The first velocity peak is attributed to the leading dilatational field lobe, which encircles the supershear rupture tip (Mello et al., 2010). The second velocity peak which follows immediately is accurately correlated to the arrival of the shear Mach front. The fault parallel signal eventually reaches a steady sliding value of around 2 m/s resulting in a crack-like rupture unlike the Denali event. The fault normal signal also features a strong trailing Rayleigh pulse, shaded in blue in Fig. 3F, which follows immediately after the passage of the shear Mach cone peak. The arrival of this strong pulse is very well correlated with the visual evidence of the arrival of the trailing Rayleigh pulse fringe concentration at the measuring station (Figs. 3D, E).

Fig. 4 shows the comparison between the scaled laboratory ground motion records, using the scaling arguments developed earlier, and the actual Denali PS10 ground motion records. Each point labeled A'–H' in the laboratory particle velocity records has a corresponding point A–H in the PS10 ground motion records and vice versa. Apart from the fact that the experimental record is crack-like, the scaled records match up remarkably well with the PS10 ground motion records and capture all of the prominent signatures. The other remarkable observation is the consistency in the polarity of the laboratory velocity records when compared with the PS10 records. The dominance of the fault parallel component over the fault normal component (A vs. B) and (A' vs. B') is observed in the early portion of the experimental records although the exact level of 1.5× ratio exhibited by the PS10 records was not captured by the experimental records. Note that the PS10 fault parallel record does not exhibit a dilatational field peak prior to the arrival of the shear Mach front. This could be attributed to the fact that the lab experiment is still largely 2D-like in that there is no significant spatial variation of the rupture through depth. This point is bolstered by the results of the dynamic 3D calculations by Dunham and Archuleta (2004) which do not distinguish between the leading dilatational field and the shear Mach front. The experimental fault normal record also exhibits some striking similarities with the corresponding PS10 record between the points labeled $C' \rightarrow D' \rightarrow E'$ in the laboratory FN record and the corresponding velocity swings spanning from $C \rightarrow D \rightarrow E$ in the PS10 FN ground motion record. The magnitude of the relative velocity swings between $C' \rightarrow D'$ and $C \rightarrow D$ were forced to match as part of the scaling process. This then established the amplitude scaling which was applied to the fault parallel and vertical records. As noted by Dunham and Archuleta (2004) the almost antisymmetric nature of this part of the record at PS10 reveals that the trailing Rayleigh disturbance was pulse-like. However, since a crack-like rupture resulted in the experiment, the trailing Rayleigh disturbance failed to completely heal and hence the record is not purely antisymmetric. Nevertheless, the result captures the same general features and sense of motion observed in the corresponding portion of the PS10 fault normal ground motion record, and provides strong experimental confirmation that this portion of the PS10 record was indeed attributed to the passage of a trailing Rayleigh pulse. There is also a very nice match between the vertical record obtained in the laboratory earthquake spanning between the points $F' \rightarrow H'$. and the PS10 ground motion record spanning the interval defined by between the points labeled $F \rightarrow H$.

Bizzarri et al. (2010) noted that there was no elevation of the 5% damped response spectral accelerations in the period band 0.05–0.4 s compared to the spectral acceleration observed at non-Mach pulse stations for earthquakes that went supershear (except for a small subset of Imperial Valley stations). To check if this is observed in the laboratory experiments we also calculate the Fourier amplitude spectra (FAS) of the velocity amplitude for both the Denali Pump Station 10 record and scaled laboratory particle velocities record. To make proper comparison between the PS10 and the scaled laboratory velocity records we first resampled the scaled laboratory record at the PS10 sampling rate (100 Hz) and then applied half-cosine taper to the last 10% of the signal. The results (frequency range between 0.01 and 20 Hz) are shown in Fig. 5. First of all we note that the fault normal (FN) spectra are remarkably similar as expected because of similar rise times of the significant pulses (B, C, D) in the PS10 record and the scaled record (B', C', D'). The modest difference in the vertical (V) record is mainly due to the fact that the significant pulses in the lab record (F', G', H') have sharper peaks than their counterparts in the PS10 record (F, G, H).

The biggest difference is seen in the fault parallel (FP) record around 2.5 Hz, and beyond, as noted by Bizzarri et al. (2010). The significant difference here is clearly the lack of the precursory dilatational field (part of the velocity field carrying $\vec{\nabla} \cdot \vec{v}$ like motion) in the PS10 record. We note that this field actually represents the volumetric strain rate (first invariant of the strain rate tensor) i.e. $\vec{\nabla} \cdot \vec{v} = \dot{\varepsilon}_{xx} + \dot{\varepsilon}_{yy} + \dot{\varepsilon}_{zz}$. In the supershear regime even though the

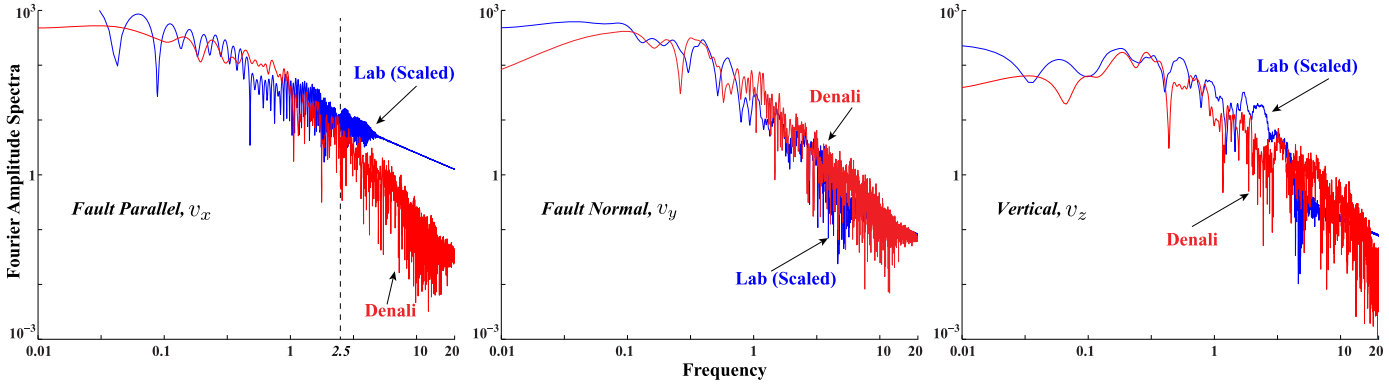

Fig. 5. Fourier amplitude spectra (FAS) of the Denali Pump Station 10 record and scaled laboratory particle velocities.

dilatational wave field is not being shocked it is approaching conditions close to it and consequently variations in the volumetric strain rate increases quite dramatically. In soils and brittle materials, like rocks, this, possibly dynamic, variations in volumetric strain rates will invariably lead to non-linear response (in soils) or comminution (in rocks). We strongly suspect this is the reason why this dilatational field was never recorded at PS10 and hence the lack of elevation of the 5% damped response spectral accelerations in the period band 0.05–0.4 s.

Nevertheless, the fact that scaled dynamic rupture experiments in brittle polymeric surrogates are capable of qualitatively reproducing all the significant features of the PS10 record is simply remarkable. It suggests that at near-source distances the strong singular elastodynamic nature of both the supershear and the trailing Rayleigh pulses swamp the near-source velocity field and the inherent inhomogeneities of the earth's crust do not contribute much to the dominant features of the ground motion.

The laboratory earthquake and the near-fault measurements presented here should thus be viewed as faithful physical analogs to the Denali event and to the resulting PS10 ground motion records. The overall goal was to reproduce the supershear portion of the Denali rupture in a controlled and repeatable laboratory setting to capture the prominent supershear ground motion signatures and to offer a strong physical basis for the design of the experiment and the interpretation of the results. All of this was possible over 6 orders of magnitude of length scale difference between the field and the experiment. Viewed from this perspective, the analog experiments were quite successful in capturing the field reality and have performed better in many respects to the best available forward and direct numerical modeling attempts offered up to this time. The success of this approach establishes controlled, scalable experiments as credible physical analogues to field events and demonstrates their value in routinely investigating near-field ground shaking signatures in the laboratory. The lack of dense enough near-source ground motion records makes their potential value only stronger.

The direct practical consequence of the above observations are that a near field station will first experience the primary fault parallel (FP) shaking due to the arrival of the supershear rupture fields, followed by a primary fault normal (FN) shaking linked to the trailing Rayleigh pulse. Structures located near a fault hosting such a transition will effectively experience two separate, closely timed earthquake events characterized by different forms of ground-shaking (one dominated by the fault parallel component and the other by the fault normal component). The timing between these two occurrences will depend on the location of the near field station relative to the point of sub-Rayleigh-to-supershear transition. Indeed, in the future, we envision the use of such analogue experiments and scaling arguments in providing accurate and scalable ground shaking records to be used as inputs to large scale structural integrity calculations in assessing the seismic hazard of realistic buildings.

Acknowledgements

The authors gratefully acknowledge the National Science Foundation for the research grant (Award No. EAS-0911723) provided under the American Recovery and Reinvestment Act (ARRA) of 2009 (Public Law 111-5). H.S.B. thanks Amaury Vallage for help provided in preparing Fig. 1. The authors are grateful to Eric Dunham and one anonymous reviewer for their helpful comments.

Appendix A. Supplementary material

Supplementary material related to this article can be found online at http://dx.doi.org/10.1016/j.epsl.2013.11.030.

References

Bizzarri, A., Dunham, E.M., Spudich, P., 2010. Coherence of Mach fronts during heterogeneous supershear earthquake rupture propagation: Simulations and comparison with observations. J. Geophys. Res. 115, B08301.

Bouchon, M., Karabulut, H., Bouin, M.-P., Schmittbuhl, J., Vallée, M., Archuleta, R., Das, S., Renard, F., Marsan, D., 2010. Faulting characteristics of supershear earthquakes. Tectonophysics 493 (3), 244–253.

Das, S., 2007. The need to study speed. Science 317 (5840), 905–906.

Dunham, E.M., Archuleta, R.J., 2004. Evidence for a supershear transient during the 2002 Denali fault earthquake. Bull. Seismol. Soc. Am. 94, S256–S268.

Dunham, E.M., Archuleta, R.J., 2005. Near-source ground motion from steady state dynamic rupture pulses. Geophys. Res. Lett. 32, L03302. http://dx.doi.org/10.1029/2004GL021793.

Dunham, E.M., Bhat, H.S., 2008. Attenuation of radiated ground motion and stresses from three-dimensional supershear ruptures. J. Geophys. Res. 113, B08319. http://dx.doi.org/10.1029/2007JB005182.

Dunham, E.M., Favreau, P., Carlson, J.M., 2003. A supershear transition mechanism for cracks. Science 299, 1557–1559.

Ellsworth, W.L., Celebi, M., Evans, J.R., Jensen, E.G., Nyman, D.J., Spudich, P., 2004a. Processing and modeling of the pump station 10 record from the November 3, 2002, Denali fault, Alaska earthquake. In: Proceedings, 11th Int. Conf. Soil Dynam. Earthq. Eng., vol. 1, pp. 471–477.

Ellsworth, W.L., Evans, J.R., Jensen, E.G., Kayen, R., Metz, M.C., Roddick, J.W., Stephens, C.D., 2004b. Near-field ground motion of the 2002 Denali fault, Alaska, earthquake recorded at pump station 10. Earthq. Spectra 20, 597–615.

Field, E.H., Dawson, T.E., Felzer, K.R., Frankel, A.D., Gupta, V., Jordan, T.H., Parsons, T., Petersen, M.D., Stein, R.S., Weldon, R., et al., 2009. Uniform California earthquake rupture forecast, version 2 (UCERF 2). Bull. Seismol. Soc. Am. 99 (4), 2053–2107.

Haeussler, P.J., Schwartz, D.P., Dawson, T.E., Stenner, H.D., Lienkaemper, J.J., Sherrod, B., Cinti, F.R., Montone, P., Craw, P.A., Crone, A.J., Personius, S.F., 2004. Surface rupture and slip distribution of the Denali and Totschunda faults in the 3 November 2002 M 7.9 earthquake, Alaska. Bull. Seismol. Soc. Am. 94 (6B), S23–S52.

Liu, Y., Lapusta, N., 2008. Transition of mode ii cracks from sub-Rayleigh to intersonic speeds in the presence of favorable heterogeneity. J. Mech. Phys. Solids 56 (1), 25–50.

Lu, X., 2009. Combined experimental and numerical study of spontaneous dynamic rupture on frictional interfaces. Ph.D. thesis. California Institute of Technology.

Lu, X., Lapusta, N., Rosakis, A.J., 2007. Pulse-like and crack-like ruptures in experiments mimicking crustal earthquakes. Proc. Natl. Acad. Sci. USA 104 (48), 18931–18936.

Mello, M., Bhat, H.S., Rosakis, A.J., Kanamori, H., 2010. Identifying the unique ground motion signatures of supershear earthquakes: Theory and experiments. Tectonophysics 493, 297–326. http://dx.doi.org/10.1016/j.tecto.2010.07.003.

Nielsen, S.B., Carlson, J.M., 2000. Rupture pulse characterization: self-healing, self-similar, expanding solutions in a continuum model of fault dynamics. Bull. Seismol. Soc. Am. 90 (6), 1480–1497.

Rice, J.R., Sammis, C.G., Parsons, R., 2005. Off-fault secondary failure induced by a dynamic slip pulse. Bull. Seismol. Soc. Am. 95 (1), 109–134.

Rosakis, A.J., 2002. Intersonic shear cracks and fault ruptures. Adv. Phys. 51, 1189–1257.

Rosakis, A.J., Xia, K.W., Lykotrafitis, G., Kanamori, H., 2007. Dynamic shear rupture in frictional interfaces: Speeds, directionality and modes. In: Kanamori, H. (Ed.), Treatise in Geophysics, vol. 4, pp. 153–192.

Samudrala, O., Huang, Y., Rosakis, A.J., 2002. Subsonic and intersonic shear rupture of weak planes with a velocity weakening cohesive zone. J. Geophys. Res. 107 (B8). http://dx.doi.org/10.1029/2001JB000460.

Xia, K.W., Rosakis, A.J., Kanamori, H., 2004. Laboratory earthquakes: The sub-Rayleigh-to-supershear rupture transition. Science 303, 1859–1861.

Supplementary Material for

Reproducing The Supershear Portion Of The 2002 Denali Earthquake Rupture In Laboratory

M. Mello, H. S. Bhat, A. J. Rosakis, H. Kanamori

1. Development of the Scaling Relationship

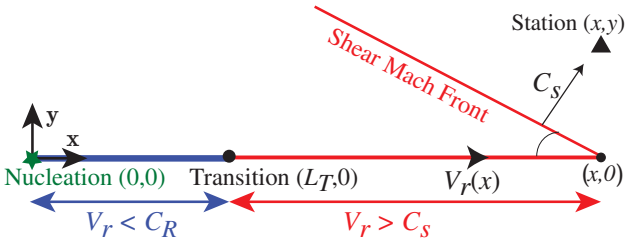

Figure 1: Problem Geometry

Consider the problem geometry shown in Fig. 1. We have a fault (horizontal straight line) where the rupture nucleates at the origin and transitions to supershear speed at $x = L_T$. The station is located at (x,y). Let $V_r(x)$ be the rupture velocity history on the fault where $V_r(x) < C_R$, the Rayleigh wave speed, for $x < L_T$ and $V_r(x) > C_s$, the shear wave speed, for $x \geq L_T$. Then the time taken for the rupture to arrive at $(x,0)$ is simply:

$$\int_0^{L_T} \frac{dx}{V_{r,SR}(x)} + \int_{L_T}^{x} \frac{dx}{V_{r,SS}(x)} \tag{1}$$

We have intentionally written the integral in the above form so that the sub-Rayleigh (SR) and the supershear (SS) parts of the rupture are separated.

By the time the rupture arrives at $(x,0)$ it is already supershear and has a Mach front associated with it. Assuming that the rupture speed is constant after transition, the Mach front is straight and the speed of the normal to the Mach front is the shear wave speed, C_s (see figure above). As an aside, note that if the rupture front accelerates or decelerates the Mach front is convex or concave respectively and the speed of the normal to the local tangent of the Mach front is still the shear wave speed. Thus the time taken for the Mach front to reach the station is simply $y\cos\theta/C_s$ where $\sin\theta = C_s/V_{r,SS}$. Thus the time taken for the main rupture information to reach the station, t_{SS}, is given by

$$t_{SS} = \int_0^{L_T} \frac{dx}{V_{r,SR}(x)} + \frac{x - L_T}{V_{r,SS}} + \frac{y\cos\theta}{C_s} \tag{2}$$

Lets now consider the time taken for the trailing Rayleigh pulse of a supershear rupture to arrive at the station. We can imagine that this pulse existed from the nucleation site and traveled at the speed of the main rupture until transition point. From here on this pulse travelled exactly at the Rayleigh wave speed, C_R. Also, lets assume that if the station is close to the fault then the pulse arrives at $(x,0)$ and the station (x,y) simultaneously i.e. the time taken for this pulse to arrive at the station (x,y) is equal to the time taken for it to propagate along the fault to a location that corresponds to the projection of the station on the fault plane, $(x,0)$. Thus the time taken for this pulse to reach the station (x,y), t_R, is,

$$t_R = \int_0^{L_T} \frac{dx}{V_{r,SR}(x)} + \int_{L_T}^{x} \frac{dx}{C_R} = \int_0^{L_T} \frac{dx}{V_{r,SR}(x)} + \frac{x - L_T}{C_R} \tag{3}$$

Hence, the difference in the rupture arrival time and the Rayleigh pulse arrival time, $\Delta t_{SS,R} = t_R - t_{SS}$, is given by

$$\Delta t_{SS,R} = \frac{x - L_T}{C_R} - \frac{x - L_T}{V_{r,SS}} - \frac{y}{C_s}\sqrt{1 - \frac{C_s^2}{V_{r,SS}^2}} \tag{4}$$

where $\cos\theta = \sqrt{1 - C_s^2/V_{r,SS}^2}$. From here on we will drop the subscript SS and simply denote the supershear rupture velocity by V_r. Solving for x we obtain,

$$x = L_T + C_s \Delta t_{SS,R} + y\sqrt{1 - \frac{C_s^2}{V_r^2}}\left(\frac{C_s}{C_R} - \frac{C_s}{V_r}\right)^{-1} \tag{5}$$

Define the following quantities,

$$\begin{aligned} \tan\beta &= \left(\frac{C_s}{C_R} - \frac{C_s}{V_r}\right)\left(1 - \frac{C_s^2}{V_r^2}\right)^{-1/2} \\ L_* &= (L_T + C_s \Delta t_{SS,R})\tan\beta \end{aligned} \tag{6}$$

Rearranging eqn. (5) and using eqn. (6) we get a linear relationship between x and y which is the locus of stations that give the same $\Delta t_{SS,R}$ given by

$$y = x\tan\beta - L_* \tag{7}$$

This locus consists of a pair of straight lines inclined at an angle $\pm\beta$ and intersecting the fault at $L_T + C_s\Delta t_{SS,R}$ (See

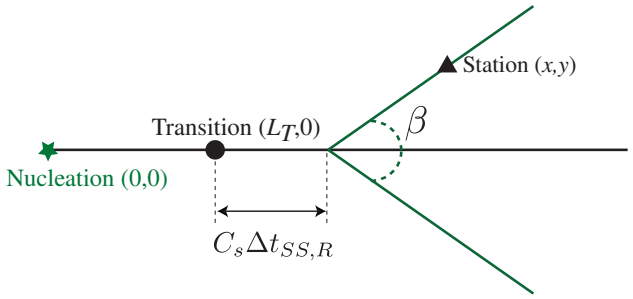

Figure 2: Locus of stations with the same $\Delta t_{SS,R}$ assuming a fixed transition length and constant supershear rupture velocity. β is defined in eqn. (6).

Fig. 2). To further constrain the above solutions we impose that geometric scaling is retained. It is assumed that in both cases, Laboratory and Denali, the ratio of the fault normal co-ordinate of the station, y, to the fault parallel distance relative to the supershear transition location, $(x - L_T)$, remain the same. That is

$$\frac{y^D}{(x^D - L_T^D)} = \frac{3\ km}{18\ km} = \frac{y^L}{(x^L - L_T^L)} = S_L \tag{8}$$

Here the superscripts D and L correspond to the Denali Pump Station 10 (PS10) and the Laboratory Station respectively. Solving the above equation with the equation for the locus, eqn. (7), we get the co-ordinates for the experimental station.

$$x^L = \frac{L_*^L - L_T^L S_L}{\tan\beta^L - S_L} \quad ; \quad y^L = S_L(x^L - L_T^L) \tag{9}$$

where

$$\begin{aligned} L_*^L &= (L_T^L + C_s^L \Delta t_{SS,R}^L) \tan\beta^L \\ \tan\beta^L &= \left(\frac{C_s^L}{C_R^L} - \frac{C_s^L}{V_r^L}\right)\left[1 - \left(\frac{C_s^L}{V_r^L}\right)^2\right]^{-1} \end{aligned} \tag{10}$$

To be very precise the above expressions determine a geometrically equivalent station, in terms of the arrival times of the rupture and the trailing Rayleigh, in a medium with different elastic properties than typical rock. One needs to know, *a priori*, the transition length, L_T^L, for the experiment (often set by a far field load level or by seeding transition by a stress perturbation) and the difference in the arrival time, $\Delta t_{SS,R}^L$.

The transition length in the laboratory is known as it is constructed by design. To determine $\Delta t_{SS,R}^L$ we make the following temporal scaling argument. We start from the Denali PS10 record which provides the equivalent time difference, $\Delta t_{SS,R}^D$. This is now scaled temporally by ensuring that the trailing Rayleigh signature in the laboratory experiment would match the same in the Denali PS10 record when multiplied by an appropriate temporal scaling factor. This requires some confidence in the constancy of the temporal width of the trailing Rayleigh signature, Δt_R^L, in the experiments. We determine Δt_R^L to be $17.8\mu s$ based on a series of past experiments which indeed show trailing Rayleigh pulses of a remarkably consistent width at near fault distances. Figure 3F of the main text indeed confirms a trailing Rayleigh pulse (shaded in blue) width of 17.8 μs as stated above. The corresponding value for Denali PS10 record, Δt_R^D is $6.9s$. Thus the temporal scaling factor, S_T, is

$$S_T = \frac{\Delta t_R^D}{\Delta t_R^L} = \frac{6.9s}{17.8\mu s} = 3.87 \times 10^5 \tag{11}$$

We can now use this temporal scaling factor to determine $\Delta t_{SS,R}^L$ based on the corresponding value for Denali PS10 i.e. $\Delta t_{SS,R}^L = \Delta t_{SS,R}^D / S_T$. Substituting this into first equation of eqn. (10) one now obtains,

$$L_*^L = \left(L_T^L + \frac{C_s^L \Delta t_{SS,R}^D}{S_T}\right) \tan\beta^L \tag{12}$$

Substituting this into eqn. (9) along with $L_T^L = 39$mm, $C_s^L = 1.28$km/s, $C_R^L = 0.92 C_s^L$ and $V_r^L = 1.7 C_s$ one obtains $(x^L, y^L) = (57, 3)$mm. Once the experimental records are obtained they are then subjected to temporal scaling using the relation, $t^{scaled} = t^L \times S_T$.